

Ultra-Compact Polarization Splitter Based on Silica Liquid Crystal Photonic Crystal Fiber Coupler

Rasha A. Hussein^{1,2}, Mohamed F. O. Hameed^{3,4}, and Salah S. Obayya³

¹ Department of Engineering Applications of Lasers
National Institute of Laser Enhanced Sciences, Cairo University, Giza, Egypt

² Department of Physics, Faculty of Science
Al-Muthana University, Muthana, Iraq
rasha.lasereng@gmail.com

³ Centre of Photonics and Smart Materials
Zewail City of Science and Technology, Sheikh Zayed District, 6th of October City, Giza, Egypt
mfarahat@zewailcity.edu.eg, sobayya@zewailcity.edu.eg

⁴ Department of Mathematics and Engineering Physics, Faculty of Engineering
Mansoura University, Mansoura, 35516, Egypt

Abstract — An ultra-compact polarization splitter based on dual core nematic liquid crystal silica photonic crystal fiber (NLC-PCF) is proposed and analyzed. The refractive index difference between the NLC and silica material guarantees the index guiding through the reported splitter. The dual core NLC-PCF has strong polarization dependence due to the birefringence between the two polarized modes. The coupling characteristics of the proposed design are studied thoroughly using full vectorial finite difference method (FV-FDM) and the propagation analysis is performed by full vectorial finite difference beam propagation method (FVFD-BPM). The numerical results reveal that the reported splitter has short device length of 482 μm with low crosstalk better than -20 dB with wide bandwidths of 31.5 nm and 19 nm for the quasi TE and quasi TM modes, respectively. The compact coupling lengths as well as the low crosstalks over reasonable bandwidths are the main advantages of the reported dual core NLC-PCF.

Index Terms — Beam propagation method, finite difference method, photonic crystal fibers, polarization splitter.

I. INTRODUCTION

The high-level integration of fiber functionalities into photonic devices is the latest trend in the development of all-fiber devices. Photonic devices based on photonic crystal fibers (PCFs) have attracted a great attention recently [1]. This is due to unique design flexibilities and optical properties of PCFs that cannot

be achieved by conventional optical fiber. In this regard, PCFs possess numerous unusual properties, such as, single-mode operation [2], high birefringence [3], controllable dispersion [4], and large mode area [5]. Moreover, the polarization properties of PCFs can be manipulated by thermo-optical responsive infiltration such as nematic liquid crystal (NLC) [6,7] into the air holes or hollow core. The NLC material is a thermotropic LC which undergoes phase transitions with temperature variation. The phase of the NLC material is changed from solid to LC state at the melting temperature T_M , and from LC to isotropic liquid state at the clearing temperature T_C . The nematic-isotropic transition of the E7 NLC material occurs at clearing temperature of 60°C. The LCs are anisotropic materials due to the tendency of the LC molecules to orient themselves along a preferred direction known as the director n . The optical anisotropy of the LC material is defined as $\Delta n = n_e - n_o$, where n_e , and n_o are the extraordinary, and ordinary refractive indices of the LC material, respectively. In addition, the refractive indices of the NLC material are temperature dependent [8]. Hence, the material anisotropy of the NLC can be tuned by changing the temperature. Moreover, the optical anisotropy is related to the polarization that occurs when an electric field is applied to the LC. For n_e the vibration vector of the plane polarized light is parallel to the director, while for n_o the vibration vector is perpendicular to the director. Hence, the optical properties of the NLC material can be changed by applying external fields [9].

Although PCFs are usually composed of central

defect surrounded by air holes arranged in regular lattice, the development of manufacturing technologies provides the ability to realize multicore PCFs as well [8,10,11]. In addition, the employment of dual core PCFs as wavelength division multiplexing (WDM) components [12], and polarization splitter [13] has been investigated. Polarization splitter can be used to separate a light signal into two orthogonal polarizations. Therefore, various PCF polarization splitters have been investigated [14-16]. In 2006, Florous, *et al.* [14] reported a polarization independent splitter which allows wavelength multiplexing at 1.3 μm , and 1.55 μm . Moreover, Hameed, *et al.* [15] proposed polarization splitter based on index guiding soft glass nematic liquid crystal PCF with device length of 8.227 mm. Furthermore, a polarization dependent coupling in dual core PCF selectively filled with gold wires has been investigated in [16].

In this paper, the polarization dependent coupling in dual core silica based PCF filled with NLC of type E7 is presented and investigated. The simulation results are obtained using full vectorial finite difference method (FV-FDM) [17] with absorbing perfectly matched layer (PML) boundary conditions [18,19] using stretched complex coordinates [20]. The beam propagation method (BPM) [21,22] can be utilized to study the field propagation along the axial direction. The propagation analysis of the suggested coupler is investigated by using full-vectorial finite difference beam propagation method (FVFD-BPM) [22]. The reported nematic liquid crystal PCF (NLC-PCF) polarization splitter guides light by modified total internal reflection (MTIR) technique, since the ordinary n_o and extraordinary n_e refractive indices of the E7 NLC are greater than that of silica background glass n_s . Further, the NLC-PCF polarization splitter has high tunability with the temperature or the applied electric field. The effect of structure parameters and temperature on the coupling characteristics of the suggested design is studied. The proposed design has short coupling length of 482 μm with crosstalk better than -20 dB. The reported splitter has bandwidths (BW) of 19 nm, and 31.5 nm for the quasi transverse magnetic (TM) and quasi transverse electric (TE) modes, respectively. The suggested splitter is different than the LC soft glass PCF coupler (LC-SGPCF) [8]. The LC-SGPCF coupler of device length 6.232 mm has a soft glass background material with a small hole of radius 0.5 μm filled with LC material. Therefore, the propagation through the region occurs around the LC central hole. However, the proposed PCF splitter in this paper has a silica background with compact device length of 482 μm with low crosstalk.

Many fabrication techniques have been implemented to realize PCF such as, stack and draw method [23], drilling [24], and sol-gel casting method

[25]. The most commonly used method is the stack and draw introduced by Knight, *et al.* [23]. Besides that, in [26] the authors have presented rapid preform connecting method using furnace of the fiber drawing tower. Additionally, various selective filling techniques are reported including UV glue sealing [27], arc fusion deformation [28], and capillary forces [29]. Moreover, Wang, *et al.* [30], presented flexible and reliable method for selective infiltration of PCF with the assistance of femtosecond (fs) laser micromachining. In this method, all cladding air holes are blocked with a section of conventional single mode fiber (SMF). Then a fs laser direct drilling is used to open the air holes selected to be filled. After that, materials such as the NLC can be infiltrated in these holes from the micro-machined fiber end by capillary action. Therefore, the authors believe that the suggested design can be fulfilled experimentally.

II. DESIGN CONSIDERATION AND NUMERICAL APPROACHES

Figure 1 depicts the proposed polarization splitter. The air holes are arranged in a triangular array in silica background with refractive index of 1.45. Dual identical cores are formed by filling two large central air holes with NLC material of type E7. The structure is basically an index guiding directional coupler since the ordinary n_o and extraordinary n_e refractive indices of the E7 NLC are greater than the refractive index of silica background. In addition, the suggested PCF can be placed between two electrodes [31] to control the orientation of the NLC director. All the cladding air holes have the same diameter and are arranged with hole pitch spacing of $\Lambda = 1.25 \mu\text{m}$. The separation between the centers of the two infiltrated cores is $\sqrt{3} \Lambda$. Moreover, the rotation angle of the E7 NLC director is taken as 0° , while the temperature is fixed at 25°C . On the other hand, n_o and n_e refractive indices of the E7 material are taken as 1.5024, and 1.6970, respectively at the operating wavelength $\lambda = 1.55 \mu\text{m}$. The relative permittivity tensor of the E7 NLC is taken as [32]:

$$\varepsilon_r = \begin{pmatrix} n_o^2 \sin^2 \varphi + n_e^2 \cos^2 \varphi & (n_e^2 - n_o^2) \cos \varphi \sin \varphi & 0 \\ (n_e^2 - n_o^2) \cos \varphi \sin \varphi & n_o^2 \cos^2 \varphi + n_e^2 \sin^2 \varphi & 0 \\ 0 & 0 & n_o^2 \end{pmatrix}, \quad (1)$$

where φ is the rotation angle of the director \mathbf{n} of the liquid crystal molecules as shown in the inset of Fig. 1. In this case, the director \mathbf{n} can be expressed as $\mathbf{n} = \cos \varphi \hat{x} + \sin \varphi \hat{y}$.

The suggested design supports even and odd modes for each of the two orthogonal polarization states. The coupling length (L_c) is one of the important parameters that is used to determine the minimum distance at which the power is transferred from one core to the other core. At a given wavelength, the L_c of the

directional coupler is given by:

$$L_C^{x,y} = \frac{\lambda}{2(n_{\text{even}}^{x,y} - n_{\text{odd}}^{x,y})}, \quad (2)$$

where $n_{\text{even}}^{x,y}$ and $n_{\text{odd}}^{x,y}$ are the effective indices of the even and odd modes, for x and y polarization, respectively, and λ is the operating wavelength.

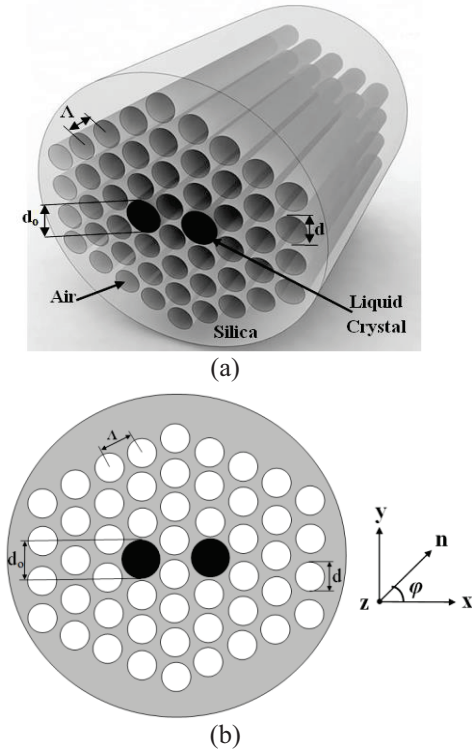


Fig. 1. The suggested dual core NLC-PCF. (a) 3D structure, (b) 2D-cross section. The director \mathbf{n} of the NLC with rotation angle φ is shown in the right.

The effective indices of the two polarized modes are calculated as follows:

First, the vector wave equation for the magnetic field vector \mathbf{H} can be derived from Maxwell's equation as follows:

$$\nabla \times (\varepsilon^{-1} \nabla \times \mathbf{H}) - \omega^2 \mu_0 \mathbf{H} = 0, \quad (3)$$

where ω is the angular frequency, μ_0 is the free space permeability and ε is the permittivity tensor of the waveguide material which is given by:

$$\varepsilon = \varepsilon_o \varepsilon_r = \varepsilon_o \begin{pmatrix} \varepsilon_{xx} & \varepsilon_{xy} & 0 \\ \varepsilon_{yx} & \varepsilon_{yy} & 0 \\ 0 & 0 & \varepsilon_{zz} \end{pmatrix}, \quad (4)$$

where ε_o is the free space permittivity, and ε_r is the relative permittivity tensor of the waveguide material. Using the divergence relation $\nabla \cdot \mathbf{H} = 0$, and the vector wave equation, one can obtain the following full vector eigenvalue equation after some algebraic manipulations:

$$\begin{bmatrix} A_{xx} & A_{xy} \\ A_{yx} & A_{yy} \end{bmatrix} \begin{bmatrix} H_x \\ H_y \end{bmatrix} = \beta^2 \begin{bmatrix} H_x \\ H_y \end{bmatrix}, \quad (5)$$

where β is the propagation constant, and the differential operators A_{xx} , A_{xy} , A_{yx} , and A_{yy} can be found in [17]. Equation (5) is the full vector eigenvalue equation which describes the propagated modes for anisotropic optical waveguides. The eigenvectors are the two transverse field components H_x and H_y , and β^2 is the corresponding eigenvalue. The effective index of the propagated mode can be calculated from β such that $n_{\text{eff}} = \beta/k$, where k is the free space wave number. The differential operators can be approximated by using FDM [17] and the robust PML boundary condition [18,19] is employed at the edges of the computational window to account for the leakage property of the modes. In this investigation, the grid sizes Δx and Δy in x and y directions, respectively are taken as $0.02 \mu\text{m}$ through all simulations.

To analyze the propagation along the suggested polarization splitter, the use of full vectorial beam propagation method [19,22,33] is mandatory. In this investigation, the FVFD-BPM [22] is used to study the propagation of the light along the propagation direction z of the suggested splitter with slowly varying envelope approximation such that $H_t = \hat{H}_t e^{-jk_0 z}$. The following two equations can then be obtained after some algebraic manipulation:

$$[1 + j\Delta z \alpha B_{xx}] \hat{H}_x^{L+1} = [1 - j\Delta z (1 - \alpha) B_{xx}] \hat{H}_x^L - j\Delta z B_{xy} \hat{H}_y^L, \quad (6)$$

$$[1 + j\Delta z \alpha B_{yy}] \hat{H}_y^{L+1} = [1 - j\Delta z (1 - \alpha) B_{yy}] \hat{H}_y^L - j\Delta z B_{yx} \hat{H}_x^L, \quad (7)$$

where n_0 is the reference index required to satisfy the slowly varying envelope approach, α is a weighting factor introduced to control the stability of the finite difference scheme. Further, B_{xx} , B_{xy} , B_{yx} , and B_{yy} are the new differential operators which are approximated using the FDM [17,22]. The required magnetic fields can be calculated by solving equations (6) and (7) for the transverse magnetic fields by an iterative procedure.

The magnetic fields \hat{H}_x^{L+1} and \hat{H}_y^{L+1} at a distance L+1 in the z-direction can be obtained from the previous magnetic fields, \hat{H}_x^L and \hat{H}_y^L , respectively at a distance L in the z-direction. In this study, the step sizes Δx and Δy are fixed to $0.02 \mu\text{m}$ while the longitudinal step size Δz is taken as $1.0 \mu\text{m}$. In this regard, Obayya, *et al.* [33] proves that the beam propagation analysis is unconditionally stable when the longitudinal step size $\Delta z \leq 1.0 \mu\text{m}$. Additionally, the reference index n_0 is taken as the effective index of the fundamental mode launched at the input waveguide. Also, α is chosen within the range, $0.5 \leq \alpha \leq 1.0$, to have unconditionally stable FVFD-BPM [22].

III. NUMERICAL RESULTS

Figure 2 shows the wavelength dependence of the coupling length of the two polarized modes at different core radii r_o , 0.625 μm , 0.65 μm , and 0.675 μm , respectively. In this study, the hole pitch Λ , cladding air hole radius r , and rotation angle are fixed to 1.25 μm , 0.525 μm , and 0°, respectively. As the wavelength increases, the modal fields will be less confined inside the NLC infiltrated cores. As a result, the distance taken by the two guided modes and hence, the coupling lengths decrease with increasing the wavelength as shown in Fig. 2. In addition, the distance between the two cores and hence, the coupling lengths decrease by increasing the core radius.

It is also noticed from Fig. 2 that the coupling length of the quasi TE mode is longer than that of the quasi TM mode at $\phi = 0^\circ$. At $\phi = 0^\circ$ the permittivity tensor of the E7 material is a diagonal of $\epsilon_r = [n_e^2, n_o^2, n_o^2]$ so $\epsilon_{xx} = n_e^2$, and $\epsilon_{yy} = n_o^2$. Therefore, the index contrast seen by the quasi TE modes is greater than that seen by the quasi TM modes. Hence, the quasi TE modes are more confined in the core region than the quasi TM modes. Thus, the quasi TM modes take shorter distance than the quasi TE modes to transfer from one core to the other. As a result, the coupling length of the quasi TM mode is shorter than that of the quasi TE mode. The coupling length of the quasi TE mode and quasi TM modes at the operating wavelength $\lambda = 1.55 \mu\text{m}$ with core radius $r_o = 0.675 \mu\text{m}$ are equal to 482 μm , and 241 μm , respectively.

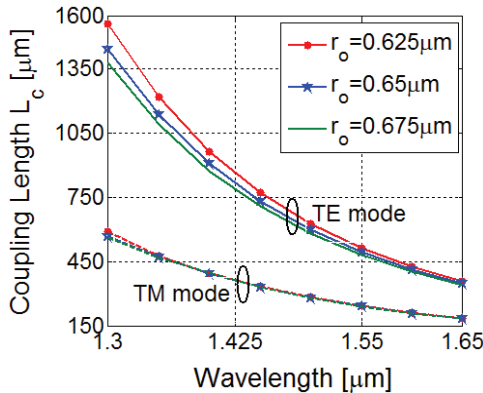


Fig. 2. Variation of the coupling length of the two polarized modes of the dual core NLC-PCF coupler with the wavelength at different core radii r_o , 0.625 μm , 0.65 μm , and 0.675 μm .

The form birefringence is defined as the ratio of the difference ($L_{CTE} - L_{CTM}$) between the coupling lengths of the quasi TE mode L_{CTE} and quasi TM modes L_{CTM} to the coupling length of the quasi TE mode L_{CTE} . The variation of the form birefringence with the wavelength at different core radii r_o , 0.625 μm , 0.65 μm , and 0.675

μm , respectively is depicted in Fig. 3. It is noted that the form birefringence decreases with increasing the core radius. As the core radius increases from 0.625 μm to 0.675 μm , the form birefringence decreases from 52.72% to 50%, respectively at the operating wavelength $\lambda = 1.55 \mu\text{m}$.

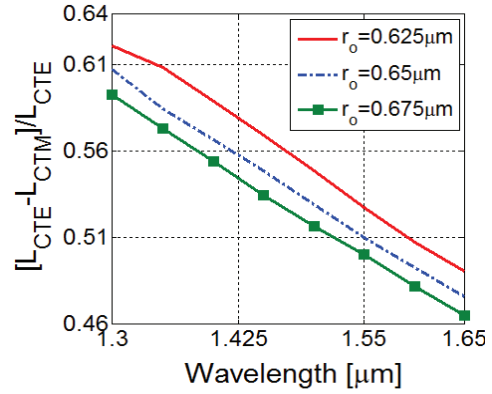


Fig. 3. Variation of the form birefringence of the dual core NLC-PCF coupler with the wavelength at different core radii r_o , 0.625 μm , 0.65 μm , and 0.675 μm .

As the ordinary n_o and extraordinary n_e refractive indices of the E7 material are temperature dependent, the effect of temperature on the coupling length of the proposed coupler is investigated. Figure 4 presents the variation of the coupling length of the two polarized modes with the temperature. In this investigation, the hole pitch Λ , core radius r_o , clad air hole radius r , rotation angle, and operating wavelength are fixed to 1.25 μm , 0.675 μm , 0.525 μm , 0°, and 1.55 μm , respectively. It is clear from this figure that the coupling length of the quasi TE mode decreases with increasing temperature while the coupling length of the quasi TM is almost constant. As the temperature increase from 15°C to 45°C, the n_e of the E7 material decreases from 1.7096 to 1.6604 at the operating wavelength $\lambda = 1.55 \mu\text{m}$. On the other hand, there is a slight change in the n_o of this material. At $\phi = 0^\circ$, ϵ_{xx} of the permittivity tensor is equal to n_e^2 , and hence, it decreases with increasing temperature. As the temperature increases, the index contrast seen by the quasi TE modes decreases, while that seen by the quasi TM modes is almost constant. Thus, the quasi TE modes will be less confined inside the core regions and accordingly the distance required by the quasi TE modes to move from one core to the other decreases with increasing the temperature. As a result, the coupling length of the quasi TE modes decreases with increasing temperature while that of the quasi TM modes is almost invariant.

The influence of the cladding air hole radius on the coupling length of the two polarized modes is examined

as shown in Fig. 5. In this study, the hole pitch Λ , core radius r_0 , rotation angle, and operating wavelength are taken as $1.25 \mu\text{m}$, $0.675 \mu\text{m}$, 0° , and $1.55 \mu\text{m}$, respectively. As the cladding air hole radius increases, the coupling lengths of the two guided modes also increase. Since the index contrast between the core and cladding regions increases, the two modes will be more confined in the core region. In addition, the silica bridge between the two cores decreases, and hence, the coupling lengths of the two guided modes increase. As the cladding air hole radius increases from the $0.5 \mu\text{m}$ to $0.575 \mu\text{m}$, the coupling lengths of the quasi TE modes arises from $433 \mu\text{m}$ to $653 \mu\text{m}$ while the coupling length of the quasi TM mode varies from $218 \mu\text{m}$ to $318 \mu\text{m}$ at the operating wavelength $\lambda = 1.55 \mu\text{m}$. It is also obvious from Fig. 5 that the suggested coupler has high birefringence, which is defined as the difference between the effective indices of the two polarized modes.

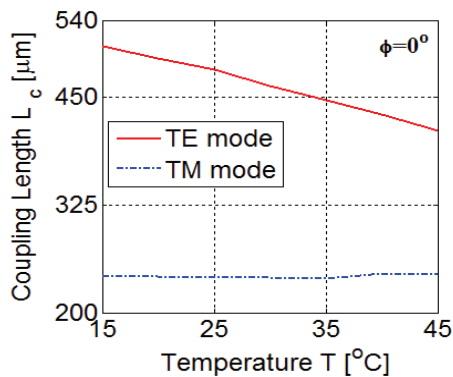


Fig. 4. Variation of the coupling length of the two polarized modes of the dual core NLC-PCF coupler with the temperature.

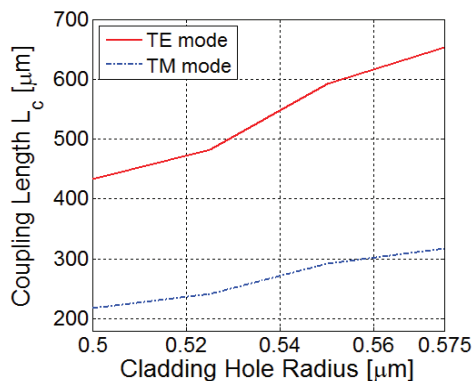


Fig. 5. Variation of the coupling length of the two polarized modes of the dual core NLC-PCF coupler with the cladding air hole radius.

The effect of the deformation of the dual infiltrated holes into elliptical cores on the performance of the proposed coupler is investigated. In this study, a_0 and b_0 are the elliptical hole radii in x - and y -directions, respectively as shown in the inset of Fig. 6. Figure 6 presents the wavelength dependence of the coupling length of the two polarized modes at different b_0 values, $0.5 \mu\text{m}$, $0.6 \mu\text{m}$, $0.675 \mu\text{m}$. In this investigation, the hole pitch Λ , cladding air hole radius r , rotation angle, and temperature are fixed to $1.25 \mu\text{m}$, $0.525 \mu\text{m}$, 0° , and 25°C , respectively. However, the radius in the x -direction a_0 is fixed to $0.675 \mu\text{m}$. It is evident from this figure that the coupling length of the two guided modes increases with increasing the b_0 value. Furthermore, the coupling length of the quasi TE mode is more affected by the variation of the b_0 value, while the coupling length of the quasi TM mode is slightly affected. Consequently, the form birefringence increases with increasing the b_0 value at constant value of a_0 as shown in Fig.7. As b_0 increases from $0.5 \mu\text{m}$ to $0.675 \mu\text{m}$, the form birefringence increases from 45.41% to 50% . At $\varphi = 0^\circ$, the index contrast seen by the quasi TE mode is greater than that seen by the quasi TM mode. Therefore, the quasi TE polarized mode will be more confined through the NLC infiltrated core. In addition, the quasi TE mode will be more affected by core deformation than the quasi TM mode. It is found that the suggested design offers short coupling lengths for the two polarized modes of $482 \mu\text{m}$, and $241 \mu\text{m}$ for the quasi TE and quasi TM modes, respectively at the operating wavelength $\lambda = 1.55 \mu\text{m}$ with $b_0 = 0.675 \mu\text{m}$. The effect of the radius a_0 in the x -direction is also studied. It is found that it has the same effect of the b_0 value on the performance of the suggested coupler.

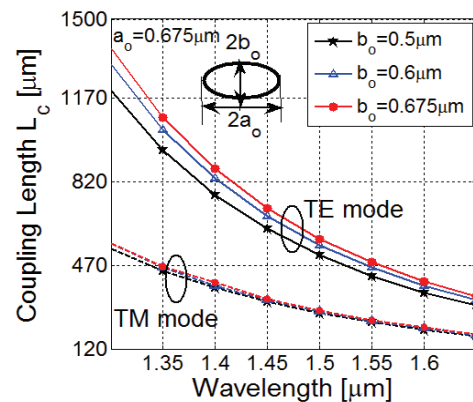


Fig. 6. Variation of the coupling length of the two polarized modes of the dual core NLC-PCF coupler with the wavelength at different b_0 values while a_0 is taken as $0.675 \mu\text{m}$.

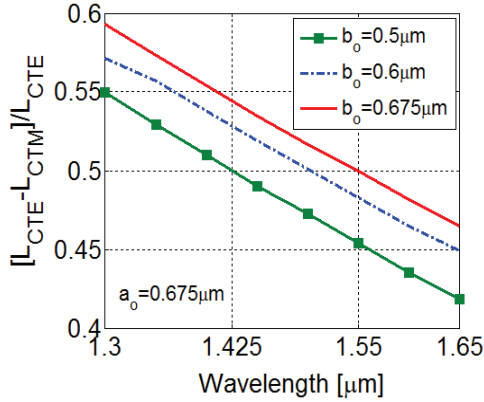


Fig. 7. Variation of the form birefringence of the dual core NLC-PCF coupler with the wavelength at different b_0 values while a_0 is taken as $0.675 \mu\text{m}$.

Figure 5 also reveals that the proposed coupler is polarization dependant due to the infiltration of NLC material that increases the birefringence between the two guided modes. Thus, the reported coupler can be used as polarization splitter. The fiber coupler can split up the two polarized states if the coupling lengths of the quasi TE and quasi TM modes satisfy the coupling ratio R [34] at a given wavelength:

$$R = L_{CTE} : L_{CTM} = i : j, \quad (8)$$

where L_{CTE} and L_{CTM} are the coupling lengths of the quasi TE and TM modes, respectively. In addition, i and j are two integers of different parities. The coupler length in this case is equal to $L_f = L_{CTM} \times i/j$. Consequently, to achieve the shortest splitter, the optimal value of R should be 2. Figure 8 presents the coupling length ratio between the L_{CTE} and L_{CTM} as a function of cladding hole radius at two different hole pitches $1.21 \mu\text{m}$ and $1.25 \mu\text{m}$, respectively. It is evident from this figure that the coupling ratio increases with increasing the cladding hole radius at specific hole pitch value. It is also shown from Fig. 8 that the coupling ratio is equal to 2 at cladding hole radius and hole pitch of $0.525 \mu\text{m}$ and $1.25 \mu\text{m}$, respectively. The L_{CTE} and L_{CTM} calculated by the FV-FDM [17] are equal to $482 \mu\text{m}$ and $241 \mu\text{m}$, respectively at the operating wavelength $\lambda = 1.55 \mu\text{m}$.

The FVFD-BPM [22] is used to confirm the polarization splitter based on the proposed coupler and to study the propagation along its axial direction. At $z = 0$, the fundamental components H_y and H_x of the quasi TE and quasi TM modes, respectively of silica PCF with one hole infiltrated with NLC obtained using FV-FDM [17] at $\lambda = 1.55 \mu\text{m}$ are launched into the left core of the reported coupler. These input fields start to transfer to the right core of the coupler and the fields are completely transferred to the right core at the corresponding coupling lengths. The coupling lengths

calculated by the FVFD-BPM are equal to $482 \mu\text{m}$ and $241 \mu\text{m}$ for the quasi TE and TM modes, respectively, which are the same values obtained by the FV-FDM. As the coupling ratio is equal to 2, therefore the length of the reported coupler is $L_f = (482 + 2 \times 241) / 2 = 482 \mu\text{m}$ at which the two polarization states are separated well.

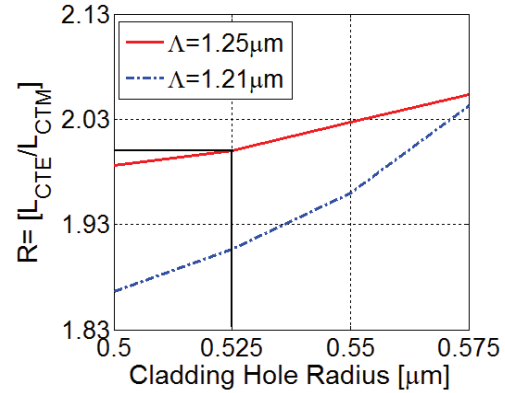


Fig. 8. Variation of the coupling length ratio for the quasi TE and quasi TM modes with the cladding hole radius at two different hole pitches $1.21 \mu\text{m}$ and $1.25 \mu\text{m}$.

Figure 9 shows the normalized power of the two polarized modes at the operating wavelength $\lambda = 1.55 \mu\text{m}$ in the left core of the suggested coupler. It is clear from this figure that the two polarized modes are separated well after a propagation distance equals to $L_f = 482 \mu\text{m}$. In addition, at $z = 482 \mu\text{m}$, the normalized power of the quasi TE mode in the right and left core of the proposed coupler are equal to 0.002056 , and 0.9979 , respectively. However, the normalized powers of the quasi TM mode in the right and left cores of the reported coupler are equal to 0.9986 , and 0.001447 , respectively.

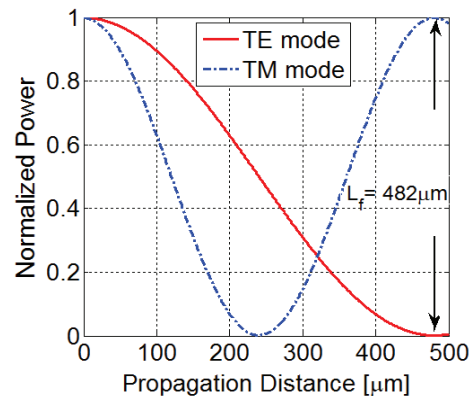


Fig. 9. Evolution of the normalized powers on the left core for the quasi TE and quasi TM modes at the operating wavelength $\lambda = 1.55 \mu\text{m}$ along the propagation direction.

The field distributions of the dominant field component H_y and H_x of the quasi TE and TM modes, respectively at the operating wavelength $\lambda = 1.55 \mu\text{m}$ are shown in Fig. 10 at different propagation distances z , 0, 241 μm , and 482 μm . At $z = 0$, the input fields are launched into the left core, and as the propagation distance increases, the normalized power in the right core increases, while that in the left core decreases. When the propagation distance is equal to the coupling length of the quasi TM mode, the normalized power of the quasi TM mode is transferred to the right core. Finally, when the propagation distance is equal to the device length L_f , the two polarized modes are separated.

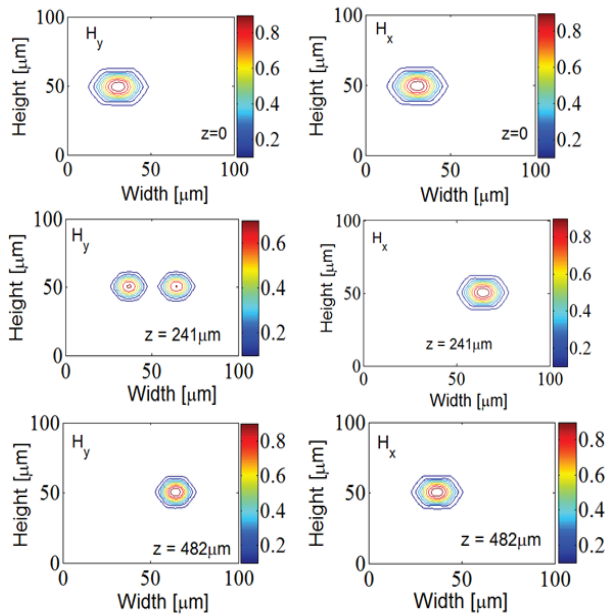


Fig. 10. Field contour patterns for H_y and H_x of the quasi TE and quasi TM modes, respectively, at z , 0, 241 μm , and 482 μm at $\lambda = 1.55 \mu\text{m}$.

One of the important parameters in designing the fiber coupler is the crosstalk, which is defined as the amount of undesired power remaining at the end of the suggested coupler. Figure 11 shows the crosstalk (CT) for the quasi TE and quasi TM modes around the operating wavelength $\lambda = 1.55 \mu\text{m}$. The crosstalk in decibel of the wanted quasi TE mode at the right core of the reported coupler is given by:

$$CT_{TE} = 10 \log_{10} \left(\frac{P_{uTM}}{P_{dTE}} \right), \quad (9)$$

where P_{dTE} and P_{uTM} are the normalized powers of the desired quasi TE and undesired quasi TM modes, respectively. However, the crosstalk of the desired quasi TM mode at the left core of the proposed coupler is defined as:

$$CT_{TM} = 10 \log_{10} \left(\frac{P_{dTE}}{P_{uTM}} \right), \quad (10)$$

where P_{dTE} and P_{uTM} are the normalized powers of the desired quasi TE and undesired quasi TM modes, respectively at the left core.

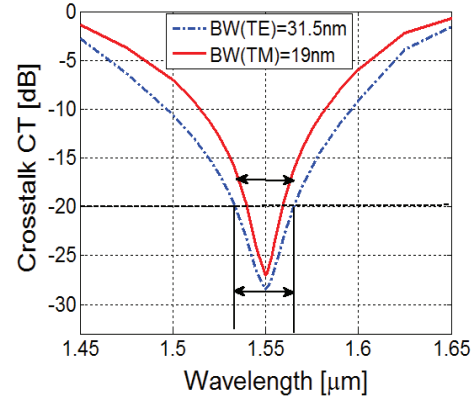


Fig. 11. Variation of crosstalk of the quasi TE and quasi TM modes of the dual core NLC-PCF coupler around the operating wavelength $\lambda = 1.55 \mu\text{m}$.

It is clear from Fig. 11 that the reported splitter has bandwidths of 31.5 nm, and 19 nm for the quasi TE and quasi TM modes, respectively at which the crosstalks are better than -20 dB. Consequently, the reported polarization splitter is less affected by the perturbation introduced during the manufacturing process due to the low level crosstalks with wide ranges of wavelength. The suggested splitter has BWs much greater than those reported in [14] and [35]. In [14], the BW is 2.0 nm around the operating wavelength $\lambda = 1.55 \mu\text{m}$, while in [35], the BW is 2.7 nm. Moreover, the proposed splitter is much shorter than those reported in [14] and [35] of lengths 15.4 mm and 9.08 mm, respectively. In addition, the dual core NLC-PCF splitter has wavelength range wider than the splitter suggested by Chen, *et al.* [34] of BW = 25.4 nm for the quasi TE mode around $\lambda = 1.55 \mu\text{m}$. On the other hand, the splitter reported in [34] has longer length of 10.69 mm than the suggested splitter. This is due to our proposed design is based on NLC core which is a birefringent material so the birefringence between the quasi TE and quasi TM modes is large as shown in Fig. 2. Hence, the quasi TE and quasi TM modes can be easily separated in a compact length. However, the reported design in the literature [34] is based on small birefringent PCF. Therefore, the coupling length [34] is greater than our design since the coupling length is inversely proportional to the birefringence as revealed from equation (2). Further, the proposed splitter is shorter than the soft glass NLC-PCF splitter reported by

Hameed, *et al.* [15] with 8.227 mm device length. Also, in [8], the authors reported soft glass PCF with dual NLC core with 6.232 mm length which is longer than the suggested splitter. Hence, the dual core NLC-PCF splitter has shorter coupling length than those reported in [8,14,15,34,35]. The proposed structure is compact in size and easy to fabricate, making it promising for miniaturized communication devices.

It should be noted that Hu and Whinnery [36] have measured the scattering losses of the bulk NLC of around 15 to 40 dB/cm. However, the scattering losses through the NLC can be decreased to 1-3 dB/cm by filling the LC into small capillaries with inner diameters less than 8 μm as reported by Green and Madden [37]. Scattering losses of 1.5 to 2.4 dB/cm [37] have been calculated along silica fiber length of 30 cm. However, the suggested NLC-PCF of device length 482 μm has two large central holes of diameter 1.35 μm filled with NLC. Therefore, low scattering losses can be obtained for our compact design.

IV. CONCLUSION

A polarization splitter based on dual core NLC-PCF coupler has been introduced and analyzed. The polarization dependent coupling is enhanced by introducing high birefringent NLC material in the two cores. The advantages of the reported splitter are the compact coupling lengths, as well as the low crosstalks over reasonable bandwidths. The suggested design has short device length of 482 μm with a crosstalk better than -25 dB with bandwidths of 31.5 nm and 19 nm for the quasi TE and quasi TM modes, respectively.

REFERENCES

- [1] K. J. Lee, K. S. Hong, H. C. Park, and B. Y. Kim, "Polarization coupling in a highly birefringent photonic crystal fiber by torsional acoustic wave," *Opt. Express*, vol. 16, no. 7, pp. 4631-4638, 2008.
- [2] T. A. Birks, J. C. Knight, and P. St. J. Russell, "Endlessly single-mode photonic crystal fiber," *Opt. Lett.*, vol. 22, no. 13, pp. 961-963, 1997.
- [3] T. P. Hansen, J. Broeng, S. E. B. Libori, E. Knudsen, A. Bjarklev, J. R. Jensen, and H. Simonsen, "Highly birefringent index-guiding photonic crystal fibers," *IEEE Photon. Technol. Lett.*, vol. 13, no. 6, 2001.
- [4] F. Shi, Y. Wu, M. Li, Y. Zhao, and L. Zhao, "Highly birefringent two-mode photonic crystal fibers with near-zero flattened dispersion," *IEEE Photonics Journal*, vol. 3, no. 6, 2011.
- [5] M. Napierała, T. Nasiłowski, E. Pawlik, F. Berghmans, J. Wójcik, and H. Thienpont, "Extremely large-mode-area photonic crystal fiber with low bending loss," *Opt. Express*, vol. 18, no. 15, pp. 15408-15418, 2010.
- [6] G. Ren, P. Shum, J. Hu, X. Yu, and Y. Gong, "Study of polarization-dependent bandgap formation in liquid crystal filled photonic crystal fibers," *IEEE Photonics Technology Letters*, vol. 20, no. 8, 2008.
- [7] M. F. O. Hameed, S. S. A. Obayya, and H. A. El-Mikati, "Highly nonlinear birefringent soft glass photonic crystal fiber with liquid crystal core," *IEEE Photonics Technology Letters*, vol. 23 no. 20, pp. 1478-1480, 2011.
- [8] M. F. O. Hameed and S. S. A. Obayya, "Coupling characteristics of dual liquid crystal core soft glass photonic crystal fiber," *IEEE J. Quantum Electron.*, vol. 47, no. 10, pp. 1283-1290, 2011.
- [9] V. A. Tolmachev, T. S. Perova, S. A. Grudinkin, V. A. Melnikov, and E. V. Astrova, "Electrotunable in-plane one-dimensional photonic structure based on silicon and liquid crystal," *Appl. Phys. Lett.*, vol. 90, 011908, 2007.
- [10] Z. Zhang, Y. Shi, B. Bian, and J. Lu, "Resonance-related coupling of symmetric dual-core hybrid photonic crystal fibers," *IEEE Photon. Technol. Lett.*, vol. 21, no. 8, pp. 525-527, 2009.
- [11] M. F. O. Hameed, S. S. A. Obayya, K. Al Begain, A. M. Nasr, and M. I. Abo ElMaaty, "Coupling characteristics of a soft glass nematic liquid crystal photonic crystal fiber coupler," *IET Optoelectronics*, vol. 3, no. 6, pp. 264-273, 2009.
- [12] M. F. O. Hameed, S. S. A. Obayya, and R. J. Wiltshire, "Multiplexer-demultiplexer based on nematic liquid crystal photonic crystal fiber coupler," *J. Opt. Quantum Electron.*, vol. 41, no. 4, pp. 315-326, 2009.
- [13] L. Zhang and C. Yang, "Polarization splitter based on photonic crystal fibers," *Opt. Express*, vol. 11, no. 9, pp. 1015-1020, 2003.
- [14] N. J. Florous, K. Saitoh, and M. Koshiba, "Synthesis of polarization independent splitters based on highly birefringent dual-core photonic crystal fiber platforms," *IEEE Photon. Technol. Lett.*, vol. 18, no. 11, pp. 1231-1233, 2006.
- [15] M. F. O. Hameed and S. S. A. Obayya, "Polarization splitter based on soft glass nematic liquid crystal photonic crystal fiber," *IEEE Photon. J.*, vol. 1, no. 6, pp. 265-276, 2009.
- [16] P. Li and J. Zhao, "Polarization-dependent coupling in gold-filled dual-core photonic crystal fibers," *Opt. Express*, vol. 21, no. 5, pp. 5232-5238, 2013.
- [17] A. B. Fallahkhair, K. S. Li, and T. E. Murphy, "Vector finite difference mode solver for anisotropic dielectric waveguides," *J. Lightwave Technol.*, vol. 26, no. 11, pp. 1423-1431, 2008.
- [18] W. C. Chew and W. H. Weedon, "A 3D perfectly matched medium from modified Maxwell's

- equations with stretched coordinates," *Microwave Optical Tech. Letters*, vol. 7, pp. 590-604, 1994.
- [19] S. Obayya, *Computational Photonics*, John Wiley & Sons, 2011.
- [20] W. C. Chew, J. M. Jin, and E. Michielssen, "Complex coordinate stretching as a generalized absorbing boundary condition," *Microwave and Opt. Technol. Lett.*, vol. 15, no. 6, pp. 363-369, 1997.
- [21] M. Rajarajan, S. S. A. Obayya, B. M. A. Rahman, K. T. V. Grattan, and H. A. El-Mikali, "Characterization of low-loss waveguide bends with offset-optimization for compact photonic integrated circuits," *Optoelectronics, IEE Proceedings*, vol. 147, no. 6, pp. 382-388, 2000.
- [22] W. P. Huang and C. L. Xu, "Simulation of three-dimensional optical waveguides by a full-vector beam propagation method," *IEEE J. Quantum Electron.*, vol. 29, no. 10, pp. 2639-2649, 1993.
- [23] J. C. Knight, T. A. Birks, P. St. J. Russell, and D. M. Atkin, "All-silica single-mode optical fiber with photonic crystal cladding," *Optics Letters*, vol. 21, pp. 1547-1549, 1996.
- [24] A. Mori, K. Shikano, K. Enbutsu, K. Oikawa, K. Naganuma, M. Kato, and S. Aozasa, "1.5 μm band zero-dispersion shifted tellurite photonic crystal fibre with a nonlinear coefficient of 675 $\text{W}^{-1}\text{km}^{-1}$," *The 30th Eur. Conf. Optical Commun. Conf.*, th. 3.3.6, 2004.
- [25] H. El Hamzaoui, L. Bigot, G. Bouwmans, I. Razdobreev, M. Bouazaoui, and B. Capoen, "From molecular precursors in solution to microstructured optical fiber: a sol-gel polymeric route," *Optical Materials Express*, vol. 1, pp. 234-242, 2011.
- [26] D. M. Chow, S. R. Sandoghchi, and F. R. M. Adikan, "Fabrication of photonic crystal fibers," *IEEE 3rd International Conference on Photonics*, 227-230, 2012.
- [27] B. T. Kuhlmey, B. J. Eggleton, and D. K. C. Wu, "Fluid-filled solid-core photonic bandgap fibers," *J. Lightwave Technol.*, vol. 27, no. 11, pp. 1617-1630, 2009.
- [28] L. Xiao, W. Jin, M. S. Demokan, H. L. Ho, Y. L. Hoo, and C. L. Zhao, "Fabrication of selective injection microstructured optical fibers with a conventional fusion splicer," *Opt. Express*, vol. 13, no. 22, pp. 9014-9022, 2005.
- [29] Y. Y. Huang, Y. Xu, and A. Yariv, "Fabrication of functional microstructured optical fibers through a selective filling technique," *Appl. Phys. Lett.*, vol. 85, no. 22, pp. 5182-5184, 2004.
- [30] Y. Wang, C. R. Liao, and D. N. Wang, "Femtosecond laser-assisted selective infiltration of microstructured optical fibers," *Opt. Express*, vol. 18, no. 17, pp. 18056-18060, 2010.
- [31] M. W. Haakestad, T. T. Alkeskjold, M. D. Nielsen, L. Scolari, J. Riishede, H. E. Engan, and A. Bjarklev, "Electrically tunable photonic bandgap guidance in a liquid-crystal-filled photonic crystal fiber," *IEEE Photon. Technol. Lett.*, vol. 17, no. 4, 2005.
- [32] G. Ren, P. Shum, X. Yu, J. Hu, G. Wang, and Y. Gong, "Polarization dependent guiding in liquid crystal filled photonic crystal fibers," *Opt. Commun.*, vol. 281, no. 6, pp. 1598-1606, 2008.
- [33] S. S. A. Obayya, B. M. A. Rahman, and H. A. El-Mikati, "New full-vectorial numerically efficient propagation algorithm based on the finite element method," *J. Lightwave Technol.*, vol. 18, no. 3, 2000.
- [34] M. Y. Chen and J. Zhou, "Polarization-independent splitter based on all-solid silica-based photonic-crystal fibers," *J. Lightwave Technol.*, vol. 24, no. 12, pp. 5082-5086, 2006.
- [35] N. Florous, K. Saitoh, and M. Koshiba, "A novel approach for designing photonic crystal fiber splitters with polarization-independent propagation characteristics," *Opt. Express*, vol. 13, no. 19, pp. 7365-7373, 2005.
- [36] C. Hu and J. R. Whinnery, "Losses of a nematic liquid-crystal optical waveguide," *J. Opt. Soc. Am.*, vol. 64, pp. 1424-1432, 1974.
- [37] M. Green and S. J. Madden, "Low loss nematic liquid crystal cored fiber waveguides," *Appl. Opt.*, vol. 28, pp. 5202-5203, 1989.